Fault lubrication and earthquake propagation in thermally unstable rocks

Nicola De Paola[1], Takehiro Hirose[2], Tom Mitchell[3], Giulio Di Toro[4,5], Cecilia Viti[6], and Toshihiko Shimamoto[7]

[1]Rock Mechanics Laboratory, Earth Sciences Department, University of Durham, South Road, Durham DH13LE, UK

[2]Kochi Institute for Core Sample Research, Japan Agency for Marine-Earth Science and Technology (JAMSTEC), 200 Monobe-otsu, Kochi 783-8502, Japan

[3]Experimental Geophysics Laboratory, Institute for Geology, Mineralogy, and Geophysics, Ruhr-University Bochum, D-44780 Bochum, Germany

[4]Istituto Nazionale di Geofisica e Vulcanologia, Via di Vigna Murata 605, Rome 00143, Italy

[5]Dipartimento di Geoscienze, Università degli Studi di Padova, Via Giotto 1, Padua 35137, Italy

[6]Dipartimento di Scienze della Terra, Università degli Studi di Siena, Via Laterina 8, Siena 53100, Italy

[7]Department of Earth and Planetary Systems Science, Graduate School of Science, Hiroshima University, 1-3-1, Kagami-yama, Higashi-Hiroshima 739-8526, Japan

ABSTRACT

Experiments performed on dolomite or Mg-calcite gouges at seismic slip rates (v > 1 m/s) and displacements (d > 1 m) show that the frictional coefficient μ decays exponentially from peak values ($m_p \approx 0.8$, in the Byerlee's range), to extremely low steady-state values ($\mu_{ss} \approx 0.1$), attained over a weakening distance D_w. Microstructural observations show that discontinuous patches of nanoparticles of dolomite and its decomposition products (periclase and lime or portlandite) were produced in the slip zone during the transient stage ($d < D_w$). These observations, integrated with CO_2 emissions data recorded during the experiments, suggest that particle interaction in the slip zone produces flash temperatures that are large enough to activate chemical and physical processes, e.g., decarbonation reactions (T = 550 °C). During steady state ($d \geq D_w$), shear strength is very low and not dependent upon normal stresses, suggesting that pressurized fluids (CO_2) may have been temporarily trapped within the slip zone. At this stage a continuous layer of nanoparticles is developed in the slip zone. For $d \gg D_w$, a slight but abrupt increase in shear strength is observed and interpreted as due to fluids escaping the slip zone. At this stage, dynamic weakening appears to be controlled by velocity dependent properties of nanoparticles developed in the slip zone. Experimentally derived seismic source parameter W_b (i.e., breakdown work, the energy that controls the dynamics of a propagating fracture) (1) matches W_b values obtained from seismological data of the A.D. 1997 M6 Colfiorito (Italy) earthquakes, which nucleated in the same type of rocks tested in this study, and (2) suggests similar earthquake-scaling relationships, as inferred from existing seismological data sets. We conclude that dynamic weakening of experimental faults is controlled by multiple slip weakening mechanisms, which are activated or inhibited by physicochemical reactions in the slip zone.

INTRODUCTION

Several thermally activated slip weakening mechanisms have been suggested in the literature to account for low frictional strength of faults during earthquake propagation: flash heating (Rice, 2006), thermal pressurization (Sibson, 1973; Rice, 2006), frictional melting (Spray, 2005; Hirose and Shimamoto, 2005; Di Toro et al., 2006), gel formation (Goldsby and Tullis, 2002; Di Toro et al., 2004), thermal decomposition (Han et al., 2007), nanopowder lubrication (Han et al., 2010), and elastohydrodynamic lubrications (Brodsky and Kanamori, 2001). During rapid slip (> 0.1 m/s, depending on asperity size and weakening temperature), flash temperatures at highly stressed frictional microcontacts (asperities) can activate chemical reactions (production of mineral phases with low friction coefficient) and physical changes (grain-size reduction, release and pressurization of gas and/or supercritical fluid) in the slip zone that may ultimately lower the friction coefficient, μ (Rice, 2006; Beeler et al., 2008). The abrupt temperature rise due to frictional heating can also lead to the rapid thermal pressurization of fluids trapped in the slip zone (Sibson, 1973; Rice, 2006). This can increase the pore fluid pressure P_f, thereby reducing the effective normal stress $\sigma_n' = \sigma_n - P_f$, leading to a reduction of the shear strength $\tau_f = \mu \times \sigma_n'$ of fault rocks for any given friction coefficient μ. Thermal pressurization mechanisms can operate on fluids already present within the slip zone and on those released by reactions activated by frictional heating during slip, e.g., dehydration (Hirose and Bystricky, 2007; Brantut et al., 2008) and decarbonation reactions (Han et al., 2007, 2010; Sulem and Famin, 2009). Chemical decomposition reactions, due to frictional heating in slip zones, can produce nanoparticles that show a strong velocity weakening dependence (powder lubrication; Han et al., 2010).

To investigate the dynamic weakening mechanisms activated during seismic slip in thermally unstable rocks, we performed 34 experiments at room temperature and humidity conditions with a high-velocity rotary shear friction apparatus (Hirose and Shimamoto, 2005). We tested dolomite gouges of the Triassic Evaporites Formation in the Northern Apennines (Italy), the source of the A.D. 1997 Colfiorito Mw ≤ 6 earthquakes (Miller et al., 2004; Mirabella et al., 2008). Seismic source parameters calculated from laboratory experiments on the selected gouges are compared with values obtained from seismic inversion analysis of the Colfiorito earthquakes (Tinti et al., 2005).

EXPERIMENTAL RESULTS

Experiments were performed on fine-grained (≈100 μm) gouges of (1) pure dolomite, (2) partially decomposed dolomite, and (3) totally decomposed dolomite (Figs. DR1 and DR2 in the GSA Data Repository[1]). A synthetic fault zone was created by sandwiching an ~1-mm-thick gouge layer between two cylindrical (25 mm in diameter) gabbro host rocks. The specimen assemblage was confined by a Teflon ring to limit gouge loss during the experiments (Mizoguchi et al., 2007) (Fig. DR2).

The experiments were run at normal stresses ranging from 0.4 to 2 MPa, slip rates of 0.009–1.3 m/s, and displacements of 0.20–58 m, while monitoring CO_2 emission rates (Supplementary Data 1 in the Data Repository). For slip rates, v > 0.69 m/s, all gouge materials (Table DR1)

[1]GSA Data Repository item 2011029, Supplementary Data 1 (CO_2 emission data), Supplementary Data 2 (microstructural observations of decomposed material), Supplementary Data 3 (CO_2 emission data, temperature rise, and slip weakening mechanisms), Figures DR1–DR3, and Table DR1 (summary of mechanical data), is available online at www.geosociety.org/pubs/ft2011.htm, or on request from editing@geosociety.org or Documents Secretary, GSA, P.O. Box 9140, Boulder, CO 80301, USA.

display a dramatic reduction in shear strength τ_f from initial peak values τ_p to steady-state value τ_{ss}, over a transient of distance D_w according to a best-fit exponential law (Fig. 1). The D_w is calculated as the displacement at which $\tau_p - \tau_f$ is 95% of $\tau_p - \tau_{ss}$ (Mizoguchi et al., 2007). For v = 1.3 m/s, CO_2 emissions have been recorded since the transient stage during experiments on both dolomite and partially decomposed dolomite (Figs. 1A–1C). Semiquantitative X-ray powder diffraction (XRPD) analyses of the entire thickness of the deformed dolomite gouge layer confirmed the presence of variable amounts of Mg-rich calcite, portlandite, and periclase (i.e., the thermal decomposition products of dolomite when $T > 550$ °C; Fig. DR3 and Supplementary Data 2). When relatively small (Fig. 1A) (or absent; Fig. 1D) amounts of CO_2 emissions have been recorded, a smooth decay trend of τ_f has been observed. On the contrary, when large amounts of CO_2 emissions have been recorded, the dynamic shear strength displays a different decay trend as two distinct steady states are attained (Figs. 1B and 1C). In these cases, a sharp increase in dynamic shear strength is suddenly observed for displacements larger than D_w, resulting in the attainment of a second steady state, $\tau_{ss2} > \tau_{ss1}$ (Figs. 1B and 1C).

MICROSTRUCTURAL OBSERVATIONS

A set of experiments was performed on dolomite gouges at constant normal stress (σ_n = 1.2 MPa) and slip rate (1.3 m/s) with different displacements d (Fig. 2A). All laboratory-deformed samples show the localization of slip at the gouge–host rock boundary, within thin slip zones (50–100 µm) formed by fine- to ultrafine-grained material (Fig. 2A; see inset). For d = 1.58 m < D_w, a thin (few tens of microns) and discontinuous slip zone developed, characterized by patches of submicron-sized clasts (average grain size ϕ_{av} = 500 nm; Figs. 2B and 2C). For d = 2.7 m < D_w, a thicker (>50 µm) and continuous slip zone developed, characterized by a continuous band of submicron-sized clasts (ϕ_{av} = 100 nm) and development of pervasive slip planes (Figs. 2D and 2E). Thick slip zones (≥100 µm) developed for d ≥ D_w. In this latter case, transmission electron microscopy observations show that the slip zone of the experimental samples is formed by a complex association of nanoparticles (ϕ_{av} = 20 nm), giving rise in places to a compact, pore-free texture, with recurrent polygonalized boundaries (Fig. 2F). Ring-shaped selected area electron diffraction patterns (see inset in Fig. 2F) indicate random crystal orientation (Figs. 2F and 2G; Supplementary Data 2). High-resolution images show that nanoparticles are formed by ordered, defect-free sequences of lattice fringes, suggesting significant structural reorganization (Fig. 2G; Supplementary Data 2).

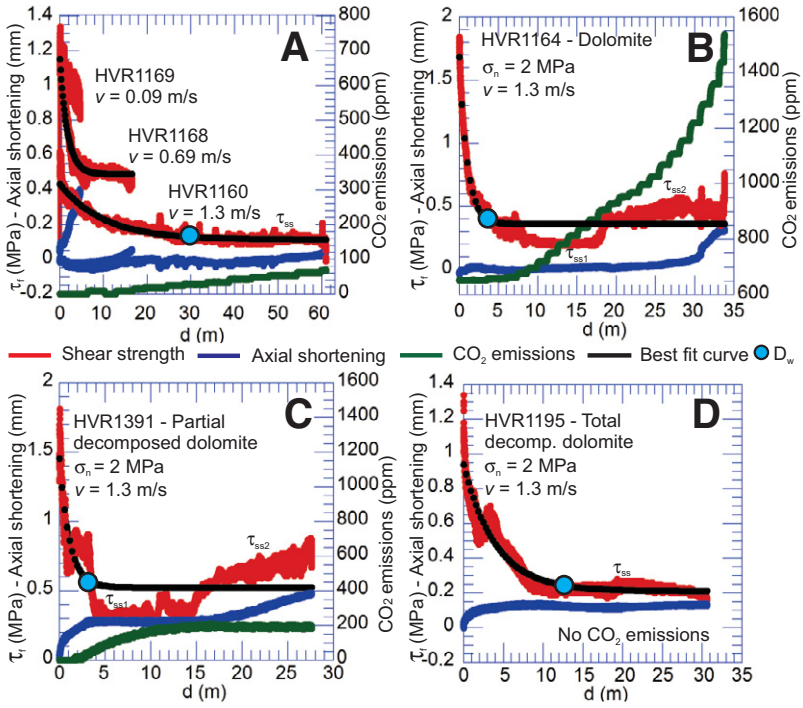

Figure 1. Low- and high-velocity (v) friction experiments data. (See text for discussion.) A: Room-humidity dolomite: for $v \geq 0.69$ m/s, τ_f is fitted by exponential decay law $\tau_f = \tau_{ss} + (\tau_p - \tau_{ss})e^{[\ln(0.05)d/Dw]}$ from peak (τ_p) to steady-state(τ_{ss}) values when plotted versus displacement (Mizoguchi et al., 2007). Steady-state shear strength is within Byerlee's range for low slip rates and becomes extremely low for $v \geq 1.3$ m/s. Slip weakening distance D_w is plotted on best-fit curve for each diagram. Very small amounts of CO_2 emissions were recorded during experiment. B: Room humidity dolomite. C: Partially decomposed dolomite. For B and C, τ_f displays trend similar to that shown in A, but here attains two steady-state values with $\tau_{ss2} > \tau_{ss1}$. Axial shortening was small during experiment. In both cases, CO_2 emissions were recorded toward end of transient phase. D: Totally decomposed dolomite: τ_f displays trend similar to that shown in B and C, but here only one steady-state value τ_{ss} is attained.

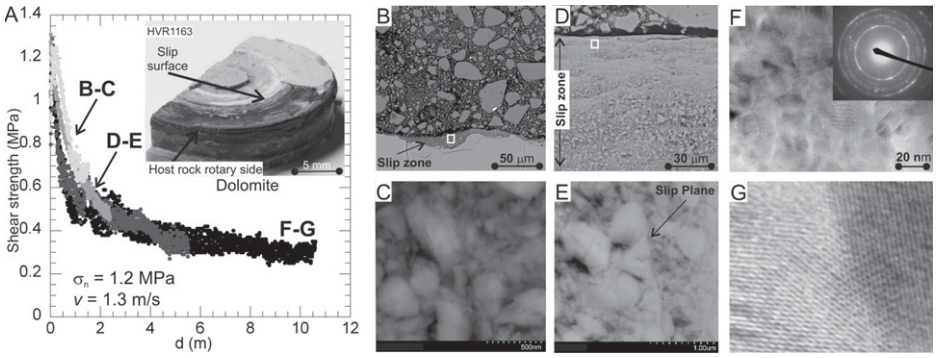

Figure 2. Mechanical data and microstructures of deformed room-humidity dolomite gouge. A: τ_f versus displacement, d, diagram (see text) showing evolution of shear strength for experiments arrested at different values of d. Inset shows localized slip zone developed within deformed gouge layer at contact with host rock (rotary side). B: Scanning electron microscopy (SEM) picture showing discontinuous and weakly developed slip zone for d = 1.58 m < D_w. C: High-magnification SEM picture of area highlighted by white box in slip zone of B shows isolated patch of submicron material. D: SEM picture showing well-developed slip zone for d = 2.7 m < D_w. E: High-magnification SEM picture of area highlighted by white box in slip zone of D showing slip surfaces within continuous bands of nanoscale material, extending subparallel to main slip zone. F: Transmission electron microscopy (TEM) image of slip zone developed for d >> D_w: rounded to polygonalized grains to 20 nm in size, producing compact, pore-free nanotextures. Inset: Corresponding ring-shaped selected area electron diffraction pattern. G: Detail of F: ordered, defect-free sequences of ~3A spaced (104) lattice fringes in nanograins.

DISCUSSION

Figure 3A shows the shear versus normal stress data for the entire set of experiments performed. The (lower) steady-state dynamic shear strength values τ_{ss1} show little dependence on the normal stress; on the contrary, the (higher) steady-state dynamic shear strength values τ_{ss2} increase for increasing σ_n (Fig. 3A). This can be explained for $d >> D_w$ by the increase of the effective normal stress $\sigma'_n = \sigma_n - P_f$, if pressurized CO_2 escapes from the localized slip zone and P_f is reduced, resulting in $\tau_{ss2} = \mu_{ss}(\sigma_n - P_{f2}) > \tau_{ss1} = \mu_{ss}(\sigma_n - P_{f1})$ for $P_{f1} > P_{f2}$. For $d \leq D_w$, the Teflon ring seal and the permeability of the host rock and gouge layer may limit the CO_2 emission rates; for larger displacements ($d >> D_w$), the CO_2 emission rates keep increasing as the CO_2 pressure within the gouge layer may largely overcome the confinement exerted by the Teflon ring (Figs. 1B and 1C). In the absence of direct measurements of P_f during the experiments, we favor the former interpretation based on the following observations: (1) the attainment of two steady states was never observed during experiments where there were no CO_2 emissions (Fig. 1; Table DR1); (2) overall, when plotted on a τ versus σ_n diagram, the τ_{ss1} values show a weak or absent dependence to σ_n. The latter case would be expected if the effective normal stress principle applied (Fig. 3A). Following our interpretation of the data plotted in Figure 3A, thermal pressurization contributed to dynamic weakening during the transient stage of frictional strength decay. However, thermal pressurization was not the only dynamic weakening process in operation during our experiments, as similar weakening trends have been observed for experiments where CO_2 emissions were not significant (Fig. 1A) or absent (Fig. 1D).

The frictional strength of experimental faults is velocity dependent as dynamic friction coefficient μ_{ss} decreases, with increasing velocity, from peak values of $\mu_p \approx 0.8$, in the Byerlee's range, to very low values of $\mu_{ss} \approx 0.1$, according to a best-fit power law (Fig. 3B). The integration of CO_2 emission data and temperature rise calculations (Supplementary Data 3) shows that the slip zone bulk temperature is too low to initiate the dolomite and Mg-calcite thermal decomposition reactions (Fig. 3B). This implies that during the transient stage, flash temperature rise (Rice, 2006) above the value necessary to activate the thermal decomposition of dolomite (T = 550 ºC) has been locally reached at highly stressed frictional microcontacts (Fig. 3B). Flash heating processes will produce reaction products, i.e., Mg-calcite + periclase and lime + periclase, which have very low dynamic frictional strength at our experimental conditions (Figs. 1C and 1D). The integration of mechanical, microstructural, and XRPD analyses suggest that during the transient stage ($d < D_w$) the most likely and dominant weakening mechanisms to operate were flash heating and thermal pressurization. During the transient stage, the production of nanoparticles in the slip zone, due to shear heating–activated mechanical and chemical processes, may also have contributed to reduce the frictional strength of the tested material (Han et al., 2010); although our microstructural observations show that a continuous layer of sheared nanoparticles will only develop when d approaches D_w (Fig. 2).

During the attainment of the first steady state, τ_{ss1} for $d > D_w$, dynamic weakening should mostly be controlled by velocity dependent nanoparticle lubrication processes and thermal pressurization. In fact, flash temperature rise of T = 550 ºC, at our experimental conditions, can only be maintained in those portions of the slip zone where grain size is above a critical contact dimension for which $v > v_w$ (Fig. 3C), where v_w is the critical weakening velocity for the operation of flash heating processes (Rice, 2006; Beeler et al., 2008). Microstructural observations show that when d approaches D_w, a continuous layer of nanoparticles is developed in the slip zone (Fig. 2); here flash-heating processes would significantly reduce as $v < v_w$ (Fig. 3C). During the attainment of the second steady state, τ_{ss2} for $d >> D_w$, when fluids could escape the slip zone, dynamic weakening should mostly be controlled by velocity-dependent nanoparticle lubrication processes. Han et al. (2010) proposed that nanomaterials possess a strong velocity weakening behavior.

The seismic source parameters D_w and breakdown work W_b (i.e., the energy that controls the dynamics of a propagating fracture; Tinti et al., 2005) for room humidity and saturated and partially decomposed dolomite, respectively, have been calculated from the experimental data (Figs. 4A and 4B). At seismic slip rates of 1.3 m/s, D_w decreases with increasing normal stress according to a power law least squares best-fit equation (Fig. 4A) and are not dependent on final amount of slip. Experimental D_w values are slightly higher than those obtained from dynamic modeling of the seismological data of the Colfiorito earthquakes (Fig. 4A; Tinti et al., 2005), which nucleated in the same rocks tested in this study (Mirabella et al., 2008; De Paola et al., 2008). When extrapolated at seismogenic depths (σ_n = 20–90 MPa), experimental D_w data are well within the range of seismological values (0.3–1 m), suggesting that scales of observations between experimental measurements and seismological modeling match (Fig. 4A). The calculated W_b data from the experiments are in the range of 0.7–5 MJ/m^2, within the same order of magnitude of the range of values (0.8–2.28 MJ/m^2) estimated for the Colfiorito earthquakes (Tinti et al., 2005) (Fig. 4B). The best fit to W_b data, when plotted versus the slip weakening distance D_w, is given by a power law relationship (Fig. 4B). This is similar to that inferred from seismic inversion analyses of seismological data for well-studied moderate to large earthquakes (Rice, 2006), including the Colfiorito earthquakes, that assumed frictional strength decay with slip similar to our experimental data. These results suggest that independently derived experimental and seismological data point to the same type of earthquake scaling relationship. Experimental results imply that very large dynamic

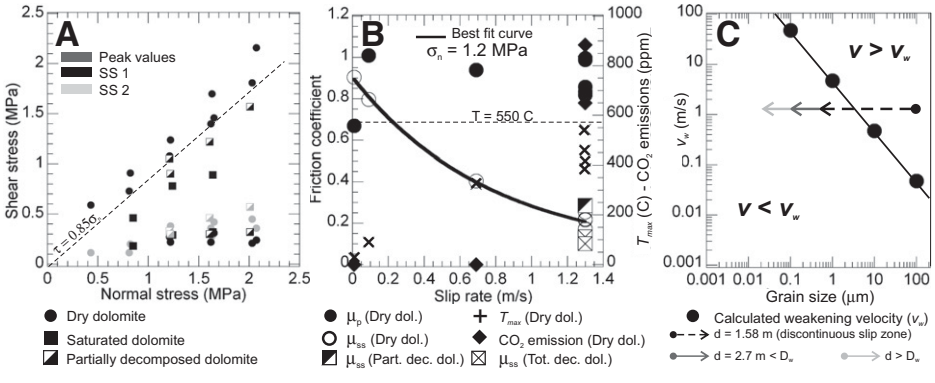

Figure 3. Measured and calculated mechanical data (see text). A: Shear versus normal stress diagram reports peak and steady-state shear stress $\tau_{ss2} > \tau_{ss1}$ for each material. Peak values are in general in agreement with Byerlee's law ($\tau_f = \mu\sigma_n$), plotted for μ = 0.85 as dashed black line. Peak shear stresses are corrected data (Table DR1; see footnote 1). B: Velocity weakening dependence of μ_{ss} fitted by exponential equation $\mu_{ss}(v) = \mu_{ss} + (\mu_p - \mu_{ss})e^{[\ln(0.05)v/v_c]}$, where μ_p is peak friction coefficient, v is velocity, and v_c = 2.31 m/s is critical velocity. CO_2 emissions and calculated T_{max} (Equation 1 in Supplementary Data 3; see footnote 1) have also been plotted versus v for experiments on dry dolomite. C: Calculated (Equation 2 in Supplementary Data 3) weakening velocity v_w versus slip zone grain size for a weakening temperature of 550 °C (decarbonation of dolomite). Flash weakening operates for $v > v_w$ and is inhibited for $v < v_w$. Arrows show evolution of grain size during experiments performed at v = 1.3 m/s and different displacements d.

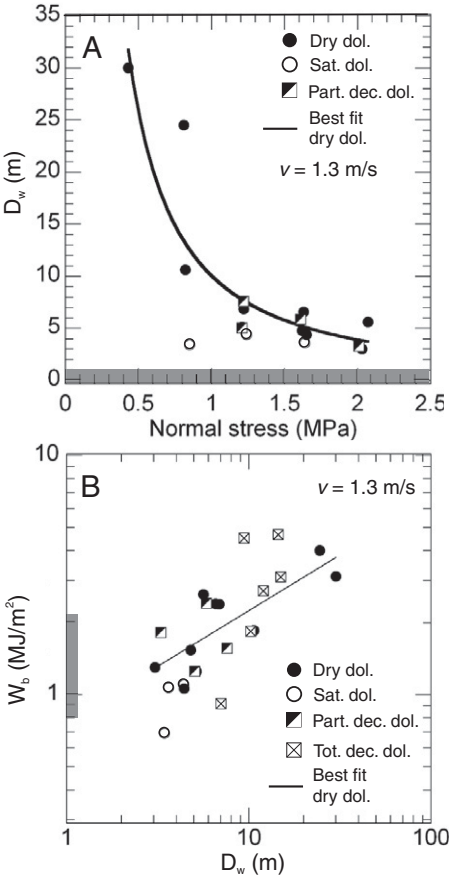

Figure 4. Calculated seismic source parameters (velocity, v = 1.3 m/s); gray boxes represent ranges of values of D_w and breakdown work W_b calculated by modeling of seismological data from A.D. 1997 Colfiorito earthquakes (Tinti et al., 2005). A: Slip weakening distance D_w versus normal stress. D_w decreases with increasing σ_n according to power law least squares best-fit equation (room-humidity dolomite): $D_w = a\sigma_n^b$; a = 10.1 and b = –1.4. B: W_b versus normal stress. W_b scales with D_w according to power law least squares best-fit equation (room-humidity dolomite): $W_b = aD_w^b$, with a = 0.77 and b = 0.47.

stress drops, of ~100 MPa, should be observed in natural earthquakes, in contrast to dynamic stress drops inferred from dynamic ground motion, which are only a few megapascals (Kanamori, 1994). This apparent paradox can be explained by assuming that the initial fault stress level can be far lower than the stress required to initiate slip, except at small patches of the fault at which rupture nucleates (Rice, 2006).

CONCLUSIONS

Experimental results show that the dynamic weakening of faults during a seismic event that propagates in thermally unstable rocks is controlled by the superimposition of multiple slip weakening mechanisms (e.g., flash heating, thermal pressurization, nanoparticle lubrication), some of which are still poorly understood (e.g., nanoparticle lubrication). During the transient decay of frictional strength from peak $\mu_p \approx 0.8$, in the Byerlee's range, to very low steady-state values, $\mu_{ss} \approx 0.1$, dynamic weakening is attained through the activation and inhibition of one or more of these mechanisms. During natural earthquake propagation, the activation and deactivation of such processes can either arrest or facilitate rupture propagation.

The seismic source parameters (D_w and W_b), calculated from the experimental results, are very close to those estimated from seismic inversion analysis for the 1997 Colfiorito earthquakes (Tinti et al., 2005), which propagated in the same rocks tested in this study and were characterized by CO_2 flux of crustal origin measured in the epicentral area after the main events (Italiano et al., 2008). Experimentally derived seismic source parameters suggest that (1) W_b scales with D_w according to a power law, in a fashion similar to that inferred from existing seismological data sets; and (2) seismogenic faults may operate at low overall stress levels apart from localized and highly stressed patches where earthquakes nucleate.

ACKNOWLEDGMENTS

De Paola acknowledges financial support from the Hiroshima University under a new education program, "Education and Training of World-Class Geoexperts." We thank N. Beeler for constructive reviews, R. Han for useful discussions on the background of this study, T. Togo for help during the experimental work, and F. Zorzi (X-ray powder diffraction analyses), L. Bowen (field emission scanning electron microscope analyses), and S. Castelli (photos). Di Toro was supported by Fondazione Cassa di Risparmio di Padova e Rovigo (CARIPARO) and a European Research Council Grant.

REFERENCES CITED

Beeler, N., Tullis, T.E., and Goldsby, D.L., 2008, Constitutive relationships and physical basis of fault strength due to flash heating: Journal of Geophysical Research, v. 113, B01401, doi: 10.1029/2007JB004988.

Brantut, N., Schubnel, A., Rouzaud, J.N., Brunet, F., and Shimamoto, T., 2008, High-velocity frictional properties of a clay-bearing fault gouge and implications for earthquake mechanics: Journal of Geophysical Research, v. 113, B10401, doi: 10.1029/2007JB005551.

Brodsky, E.E., and Kanamori, H., 2001, Elastohydrodynamic lubrication of faults: Journal of Geophysical Research, v. 106, p. 16,357–16,374, doi: 10.1029/2001JB000430.

De Paola, N., Collettini, C., Faulkner, D., and Trippetta, F., 2008, Fault zone architecture and deformation processes within evaporitic rocks in the upper crust: Tectonics, v. 27, TC4017, doi: 10.1029/2007TC002230.

Di Toro, G., Goldsby, D., and Tullis, T.E., 2004, Friction falls towards zero in quartz rock as slip velocity approaches seismic rates: Nature, v. 427, p. 436–439, doi: 10.1038/nature02249.

Di Toro, G., Hirose, T., Nielsen, S., Pennacchioni, G., and Shimamoto, T., 2006, Natural and experimental evidence of melt lubrication of faults during earthquakes: Science, v. 311, p. 647–649, doi: 10.1126/science.1121012.

Goldsby, D.L., and Tullis, T.E., 2002, Low frictional strength of quartz rocks at sub-seismic slip rates: Geophysical Research Letters, v. 29, 1844, 4 p., doi: 10.1029/2002GL015240.

Han, R., Shimamoto, T., Hirose, T., Ree, J., and Ando, J., 2007, Ultralow friction of carbonate faults caused by thermal decomposition: Science, v. 316, p. 878–881, doi: 10.1126/science.1139763.

Han, R., Hirose, T., and Shimamoto, T., 2010, Strong velocity-weakening and powder lubrication in simulated carbonate faults at seismic slip rates: Journal of Geophysical Research, v. 115, B03412, doi: 10.1029/2008JB006136.

Hirose, T., and Bystricky, M., 2007, Extreme dynamic weakening of faults during dehydration by coseismic shear heating: Geophysical Research Letters, v. 34, L14311, doi: 10.1029/2007GL030049.

Hirose, T., and Shimamoto, T., 2005, Growth of a molten zone as a mechanism of slip weakening of simulated faults in gabbro during frictional melting: Journal of Geophysical Research, v. 110, B05202, doi: 10.1029/2004JB003207.

Italiano, F., Martinelli, G., and Plescia, P., 2008, CO_2 degassing over seismic areas: The role of mechanochemical production at the study case of central Apennines: Pure and Applied Geophysics, v. 165, p. 75–94, doi: 10.1007/s00024-007-0291-7.

Kanamori, H., 1994, Mechanics of earthquakes: Annual Review of Earth and Planetary Sciences, v. 22, p. 207–237, doi: 10.1146/annurev.ea.22.050194.001231.

Miller, S.A., Collettini, C., Chiaraluce, L., Cocco, M., Barchi, M.R., and Kaus, B., 2004, Aftershocks driven by a high pressure CO_2 source at depth: Nature, v. 427, p. 724–727, doi: 10.1038/nature02251.

Mirabella, F., Barchi, M.R., Lupattelli, A., Stucchi, E., and Ciaccio, M.G., 2008, Insights on the seismogenic layer thickness from the upper crust structure of the Umbria-Marche Apennines (central Italy): Tectonics, v. 27, TC1010, doi: 10.1029/2007TC002134.

Mizoguchi, K., Hirose, T., Shimamoto, T., and Fukuyama, E., 2007, Reconstruction of seismic faulting by high-velocity friction experiments: An example of the 1995 Kobe earthquake: Geophysical Research Letters, v. 34, L01308, doi: 10.1029/2006GL027931.

Rice, J.R., 2006, Heating and weakening of faults during earthquake slip: Journal of Geophysical Research, v. 111, B05311, doi: 10.1029/2005JB004006.

Sibson, R.H., 1973, Interaction between temperature and pore-fluid pressure during earthquake faulting—A mechanism for partial or total stress relief: Nature, v. 243, p. 66–68.

Spray, J.G., 2005, Evidence for melt lubrication during large earthquakes: Geophysical Research Letters, v. 32, L07301, doi: 10.1029/2004GL022293.

Sulem, J., and Famin, V., 2009, Thermal decomposition of carbonates in fault zones: Slip-weakening and temperature limiting effects: Journal of Geophysical Research, v. 114, B03309, doi: 10.1029/2008JB006004.

Tinti, E., Spudich, P., and Cocco, M., 2005, Earthquake fracture energy inferred from kinematic rupture models on extended faults: Journal of Geophysical Research, v. 110, B12303, doi: 10.1029/2005JB003644.

Manuscript received 19 May 2010
Revised manuscript received 3 August 2010
Manuscript accepted 6 August 2010

Printed in USA